

RESEARCH

Open Access



# Integrated bioinformatics analysis identifies PCSK9 as a prognosticator correlated with lipid metabolism in pancreatic adenocarcinoma

Siqi Zhou<sup>1,2†</sup>, Qiyuan Guo<sup>1,2†</sup>, Aotian Chen<sup>2†</sup>, Xihan Li<sup>1,2\*</sup> and Xiaoping Zou<sup>1,2\*</sup>

## Abstract

**Background** Pancreatic adenocarcinoma (PAAD) is the most frequent kind of pancreatic cancer (PC). Recent studies suggest that lipid metabolism facilitates tumorigenesis, disease progression, and resistance to therapy by promoting lipid synthesis, accumulation, and breakdown. Thus, exploring the lipid metabolism network could unveil novel therapeutic avenues for early detection, precision medicine, and prognostication in PAAD. This project intends to develop new lipid metabolism-related biomarkers for PAAD diagnosis and investigate the link between important genes and immune cell infiltration (ICI).

**Methods** Tissue samples from 20 PAAD patients and 20 healthy controls were obtained. Analysis were focused on the datasets GSE71729 and GSE16515, which include samples of PAAD ( $n = 161$ ) and those from healthy human tissue ( $n = 61$ ), derived from the GEO database. Knockdown of PCSK9 on PC cells were conducted by si-RNA and sh-RNA. Migration and cell functional experiments were performed to assess the role of PCSK9 in cell multiplication. Furthermore, a xenograft mouse model was employed to confirm PCSK9's function in vivo.

**Results** The expression level of Proprotein convertase subtilisin/kexin type 9 (PCSK9) is significantly elevated in tissues affected by PAAD when compared to normal tissues. Survival analyses indicated that increased PCSK9 levels are inversely related to overall and disease-free survival (DFS). PCSK9's functional annotation associated it with the cell cycle and metabolism, especially energy metabolism. Examination of ICI data determined that PCSK9 expression demonstrated an unambiguous association with the M0 macrophages, T follicular helper cells (Tfh), gamma delta T cells and activated DC, and an inverse relationship with Monocytes, CD8<sup>+</sup> T cells, memory B cells, resting CD4<sup>+</sup> memory T cells, activated NK cells and resting DC abundance. PCSK9 expression knockdown has the ability to impede PC cells' migration and proliferation.

**Conclusion** Our study identified PCSK9 as a critical gene in PAAD. Expression levels of PCSK9 varied between PAAD and normal samples. ROC analysis verified PCSK9's strong capacity to differentiate PC from normal samples. Importantly, PCSK9 expression was considerably elevated in PC cell lines and tissues. Furthermore, PCSK9 stimulates the migration and proliferation of tumor cells in vivo and vitro.

<sup>†</sup>Siqi Zhou, Qiyuan Guo and Aotian Chen contributed equally to this manuscript.

\*Correspondence:

Xihan Li  
xihanli@nju.edu.cn  
Xiaoping Zou  
zouxp@nju.edu.cn

Full list of author information is available at the end of the article



**Keywords** Pancreatic cancer, Proprotein convertase subtilisin/kexin type 9, Tumorigenesis and progression, Tumor immunotherapy

## Introduction

PAAD, recognized for its aggressive nature and elevated mortality rate, stands as the nation's fourth typically observed cause of cancer-related mortality, according to references [1, 2]. Forecasts suggest that within the next two to three decades, it is predicted to rise to the second most prevalent cause of deaths from cancer [3]. The absence of early diagnostic techniques and efficacious therapeutic options often leads to diagnoses at advanced stages for individuals with this malignancy, contributing to an annual escalation in mortality rates [2, 4]. Growing evidence indicates that abnormalities in lipid metabolism significantly contribute to cancer's genesis, progression, responsiveness to treatment, and overall prognosis. PC formation is tightly connected with lipid metabolic processes [5–7]. Lipids, essential components of all cell membranes, are nutrients that are extensively present in organelles and composed of lipids and lipoids [8]. Abnormal lipid metabolism involves cell membrane formation and lipid-mediated cell signaling [9–11]. Therefore, the discovery of novel genes and metabolic pathways associated with lipid metabolism in PC possesses the capacity to dramatically enhance early detection, therapeutic strategies, and the prognostic assessment for individuals afflicted with PAAD.

PCSK9, identified as the ninth member in the proprotein convertase series, predominantly functions through its association with low-density lipoprotein receptors (LDLRs) located on cellular membranes. This vital interaction is essential for controlling LDL catabolism and maintaining plasma LDL concentrations [12]. Recently, PCSK9's involvement in cancer has garnered significant interest, leading to a multitude of preclinical studies across various cancers such as lung, liver, and breast cancer [13–15]. Research indicates that PCSK9 significantly influences tumor development by regulating tumor cell proliferation, apoptosis, invasion, and migration [16, 17]. PCSK9 exhibits a strong association with the dynamics of CD8<sup>+</sup> T lymphocyte infiltration and activity, as well as how other immune cells behave within the tumor microenvironment. This includes influencing the migration and polarization processes of M0 macrophages [18].

On the whole, PC expression data from the publicly accessible GEO database and TCGA database were downloaded, followed by an integrated bioinformatics analysis. The application of this methodology enabled the discovery of genes with high differential expression, the delineation of functionally enriched pathways, and

the infiltration of immune cell. Upon extensive analysis, PCSK9 emerged as the most viable biomarker and therapeutic candidate. Furthermore, we looked into how PCSK9 was expressed in PC tissues and cells, and further explored the way in which PCSK9 functions in progression of pancreatic cancer through cell and animal experiments.

## Materials and methods

### Data collection and processing

The mRNA expression datasets for PAAD were obtained from the GEO database, including GSE71729 and validation datasets GSE16515 & GSE15471. (<https://www.ncbi.nlm.nih.gov/geo/>). For this study, we picked 145 primary PDAC tumor samples and 45 normal pancreatic tissue samples GSE71729. Meanwhile we utilized 16 matched pairs of tumor and normal tissue samples for external validation GSE16515. Differential gene expression analysis on the GEO cohort was conducted using the "limma", with  $|\log_2FC| > 1.0$  and adjust  $p < 0.05$ . The "affy" package in R was employed for background adjustment, normalization, and log<sub>2</sub> conversion of all GEO raw data. For each gene represented by multiple probes, expression values were consolidated into a mean value. Information pertaining to 800 genes involved in lipid metabolism (LMRGs) was gathered from the MsigDB databases (<https://www.gsea-msigdb.org/gsea/msigdb>). Additionally, we collected the consolidated and standardized pan-cancer dataset, TCGA TARGET GTEx (PAN-CAN, N=19,131, G=60,499), from the UCSC database (<https://xenabrowser.net/>). To standardize expression values, each data point underwent a logarithmic modification of  $\log_2(x + 0.001)$ .

### Human specimens

Thirty-two PC tissues were collected at Nanjing Drum Tower Hospital which was clinical college of Jiangsu University. This study was approved by the ethics committee of Jiangsu University of Medical School.

### Functional enrichment analyses

The "clusterProfiler" instrument was employed to carry out pathway analyses for the gene ontology (GO) and Kyoto Encyclopedia of Genes and Genomes (KEGG), distinguishing between patient cohorts at elevated and diminished risk levels. Furthermore, the 'GSVA' program was employed to conduct gene set variation analysis

(GSVA), which provided a better knowledge of the variability in biological processes across different clusters.

#### Candidate diagnosis marker selection

To identify potential diagnostic markers, two algorithms based on machine learning were applied to predict PAAD status. Using the "randomForest" R package, we used Random Forest (RF), an ensemble of tree-structured classifiers, to create a regression tree with minimal error. After tenfold cross-validation, genes of the highest relative significance were chosen for their predictive accuracy. The Support Vector Machine (SVM), a supervised learning technique popular in classification and regression applications, was used. To avoid overfitting, we employed Recursive Feature Elimination (RFE) to identify the most relevant genes from the metadata cohort. As a result, SVM Recursive Feature Elimination (SVM-RFE) determined the set of genes with the maximum discriminatory power. (KM) survival plots were generated using GEPIA2 (<http://gepia2.cancer-pku.cn/#index>). Using the R package "pROC", the diagnostic potential of pivotal genes in differentiating between PAAD and normal samples was assessed through the generation of ROC curves and calculation of the Area Under the Curve (AUC) values.

#### ICI analysis

The CIBERSORT analysis was executed utilizing the "Cibersort" package in R. Bar graphs were constructed to depict the distribution of various immune cell types across different specimens. The comparative analysis of immune cell composition between PAAD and healthy samples was presented via the Sangerbox platform (<http://vip.sangerbox.com/>). Additionally, a heatmap created with "corrplot" illustrated the interrelations among 22 varieties of infiltrating immune cells.

#### Small interfering RNA (siRNA)

siRNAs targeting human PCSK9 (siPCSK9-1, F-5'-CCC AAGCAAGCAGACAUUUUAU-3'; R-5'-AUAAAUGUC UGCUUGCUUGGG-3'; siPCSK9-2, F-5'-GCCAGC AAGUGUGACAGUCAU-3'; R-5'-AUGACUGUCACA CUUGCUGGC-3'; siControl, F-5'-UUCUCCGAACGU GUCACGU-3'; R-5'-ACGUGACACGUUCGGAGAA-3') siRNAs targeting specific genes were acquired from Tsingke and introduced into cells utilizing Lipofectamine 3000.

#### Lentivirus infection

Lentiviral particles carrying GFP-Puro PCSK9 small hairpin RNA (shRNA) were utilized for stable infection, we obtained stable PCSK9 knockdown cell lines.  $1.5 \times 10^5$  tumor cells were grown in 24-well plates initially.

Lentivirus containing 5  $\mu\text{g}/\text{mL}$  polybrene was added to the plate when the cell density reached half. After 12–24 h, the fresh medium was substituted for the culture medium. The infection rate was assessed after 72 h. Subsequently, stable cell lines were screened using puromycin. Confirmation of PCSK9 knockdown was achieved by Western blot analysis before proceeding with further experiments.

#### Western blotting (WB)

After lysing the samples in RIPA buffer, it underwent sonication for Western blot examination. Subsequently, the proteins were semi-dry transferred onto PVDF membranes after using 10% SDS-PAGE gel electrophoresis to separate them. Specific antibodies from Proteintech were used to detect PCSK9 and Actin proteins.

#### Cell culture

The American Type Culture Collection provided us with four human PC cell lines (AsPC-1, BxPC-3, MIAPaCa-2, and PANC-1), and the Technical University of Munich, Germany, gave us HPDE cells as a gift. These cells were grown at 37 °C in a 5% CO<sub>2</sub> environment in RPMI-1640 media supplemented with 10% fetal bovine serum (FBS).

#### Wound healing assay

PC cells were inoculated at a density of  $1 \times 10^5$  cells per well into six-well plates. After 72 h of siRNA treatment, created a linear scratch by scraping the surface with the tip of a 200  $\mu\text{L}$  pipette. Subsequently, replaced the culture medium with RPMI-1640 medium without FBS and continued culturing the cells for 24 h. Finally, photographs of the scratch were snapped at 0 and 24 h.

#### Migration assay

BxPC-3 cells were suspended in 500  $\mu\text{L}$  of RPMI-1640 media and subsequently injected at densities of  $5 \times 10^4$  and  $2 \times 10^5$  cells/well, respectively, into the top chamber. Subsequently, the cells that had penetrated the lower side of the membrane were fixed for 15 min using methanol, and then they were stained for another 15 min using 0.5% crystal violet.

#### Colony assay

Once the PC cells were counted, they were inoculated at a density of 500 cells/well into 6-well plates. After 72 h of si-PCSK9 treatment, the culture medium was removed and replaced with fresh medium, and the cells were cultured for a further 14 days. The cells were then fixed in methanol and stained with crystal violet in methanol for 20 min before the colonies were counted.

### Immunohistochemical (IHC)

The paraffin-embedded tissue sections were deparaffinized and rehydrated sequentially, followed by overnight incubation at 4 °C with anti-PCSK9 monoclonal antibody (1:200, ab195377, Abcam). Subsequently, biotinylated secondary antibodies were added and incubated for 30 min.

### Multiplex immunohistochemical (mIHC)

To identify the expression of PCSK9 and Treg cells in tumor tissues, we performed multiple immunofluorescent labeling using an immunohistochemical kit. We sequentially applied the above primary antibodies to tissue sections and incubated them with horseradish peroxidase coupled secondary antibodies and tyramide signal amplification (TSA). After each TSA procedure, the slides were treated with microwave heating. After labeling all human antigens, the nuclei were stained with DAPI. To obtain multispectral images, the stained slides are scanned using the Mantra system (PerkinElmer).

### Xenograft mouse model

Four-week-old female BALB/c nude mice were purchased from the Jiangsu University Medical College Animal Center and kept in the facility. Following the mice were grouped,  $1 \times 10^6$  BxPc-3 cells with or without PCSK9 knockdown were subcutaneously injected into their limbs. All of the mice were put to sleep at the end of the experiment, and their tumors were removed and weighed in preparation for further examination.

### Statistics

All experiments were repeated at least three times. The data were expressed as mean+SEM. R software and GraphPad Prism (version 9.0) were implemented for all statistical analyses. Receiver operating characteristic (ROC) curves were generated by using GraphPad Prism 9. The relevance between PCSK9 clinicopathological characteristics and expression was analyzed by the Chi squared ( $X^2$ ) test. Survival curves of PC patients were performed by using Kaplan–Meier analysis. And  $p$ -value < 0.05 was considered as statistically significant.

## Results

### Identifying genes with significantly different expression levels (DEGs) and functional enrichment

A total of 145 PAAD and 46 normal tissue specimens were analyzed for differential gene expression. The differentially expressed genes (DEGs) were displayed using volcano plots and heatmaps, as shown in Fig. 1A&B. There were found to be 455 DEGs in total, 277 of which were upregulated and 178 of which were downregulated, using a threshold of  $|\log_2FC| > 1$ ,  $p < 0.05$ . As demonstrated in

Fig. 1C&D, these DEGs were substantially enriched in processes which involves "extracellular matrix organization," "collagen-containing extracellular matrix," and "endopeptidase activity," as determined by GO and KEGG pathway analyses.

Next, the 455 DEGs were intersected with 800 LMRGs from the Reactome and KEGG databases to identify 20 differentially expressed LMRGs (DELMRGs), including MBOAT2, ACSL5, VDR, SQLE, FHL2, PLA2G10, FA2H, ALB, EPHX2, LIPH, HPGD, PPARG, PCSK9, SLC44A4, PLA2G1B, CD36, SERPINA6, DPEP1, GPX2, and GC. The Venn diagram illustrating this intersections shown in Fig. 1E.

### Identification of candidate hub genes via machine learning

Two machine learning methods were used to identify important genes from the 20 DELMRGs. Figure 2A depicts the impact of decision trees. The top ten genes with the greatest relative association scores, as assessed by the Random Forest algorithm, include ALB, HPGD, MBOAT2, EPHX2, FA2H, ACSL5, PCSK9, CD36, PPARG, VDR, and FHL2, as shown in Fig. 2B. Ten feature subsets in DELMRGs were obtained using the SVM-RFE algorithm (Fig. 2C–D), contain PCSK9, PLA2G10, SERPINA6, ALB, HPGD, GPX2, PLA2G1B, CD36, GC, PPARG. Subsequently, 5 overlapping characteristics between these two algorithms were selected (PCSK9, ALB, HPGD, CD36, PPARG) (Fig. 2E) for further research.

### Identified and validated PCSK9 as a critical gene signature in PAAD

Utilizing expression profile data from GSE71729, a box-plot was generated to display the expression levels of five key genes (refer to Fig. 3A). The findings revealed that PCSK9, HPGD, and PPARG were upregulated in PC, whereas ALB and CD36 were downregulated. The GSE16515 dataset from the GEO database provided external validation, confirming the initial findings (refer to Fig. 3B). Further analysis of these genes' impact on patient survival using the GEPIA database indicated that high PCSK9 expression significantly correlated with lower OS and DFS (refer to Fig. 3C–D). To assess PCSK9's diagnostic potential, ROC assays were conducted, demonstrating its robust capability to distinguish between PAAD and normal samples in GSE71729 (AUC=0.757) (refer to Fig. 3E). The samples from GSE71729 were segregated into groups of high and low expression of PCSK9, determined by the median level of expression. GSEA was then applied to explore the disparities in biological functions between these groups, as depicted in Fig. 3F–G. This research found a high enrichment in biosynthesis, cell cycle, metabolism, and the cAMP pathway. In summary,

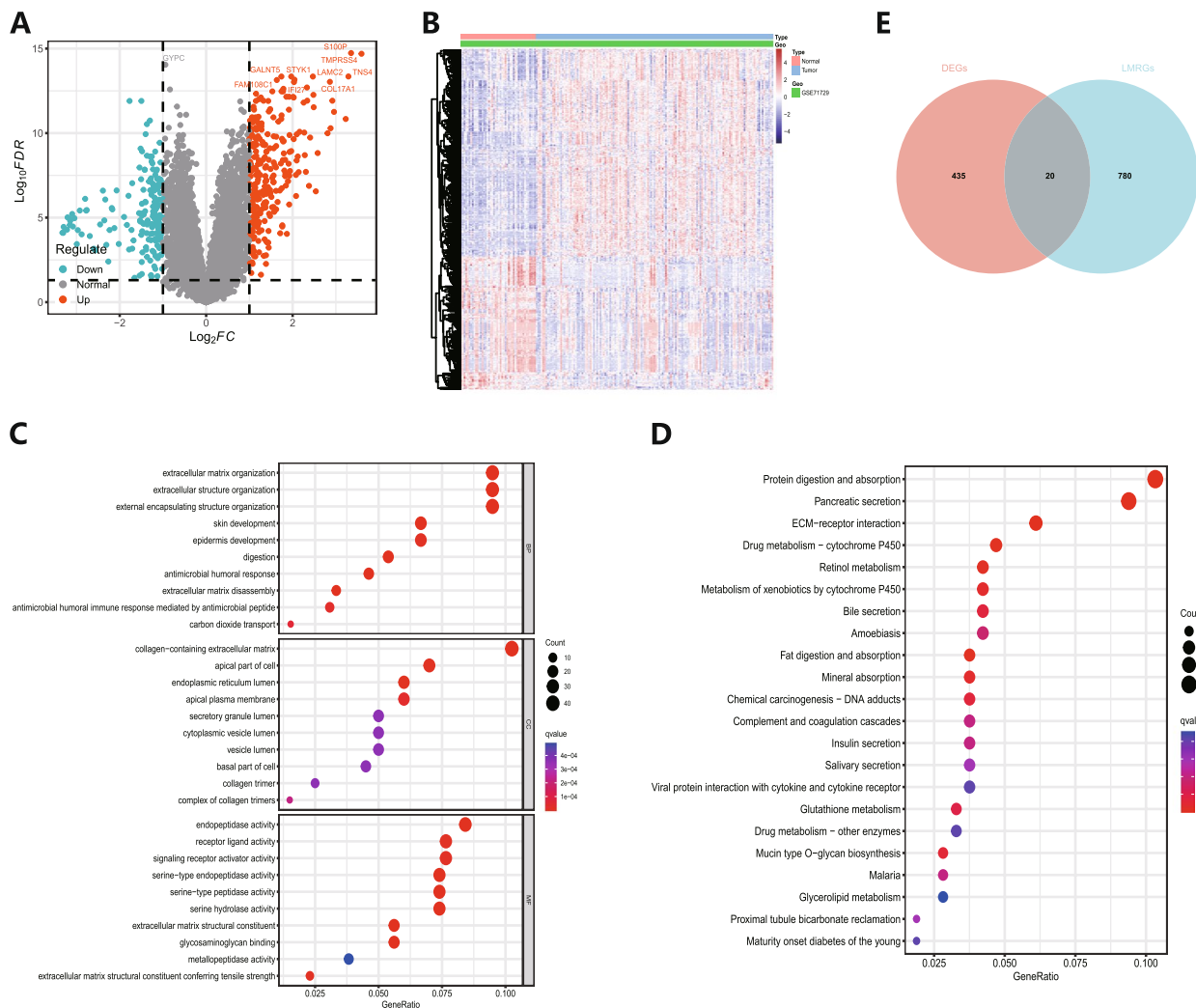


**Fig. 1** Discovery of 20 Potential Genes Associated with PC. **A** Volcano plot representing DEGs. **B** Heatmap depicting the differential expression patterns of DEGs between tumor and non-tumor tissues. **C** GO analysis outcomes for the DEGs. **D** KEGG pathway analysis results for the DEGs. **E** Overlap between the DEGs and LMRGs identified within the GEO cohort

the lipid metabolism-associated gene PCSK9 emerges as a promising biomarker for diagnosing and prognosticating PAAD.

Meanwhile, we investigated the variations in expression between tumor and normal samples from various cancer types. In 16 various tumor types—including pancreatic cancers—PCSK9 expression was noticeably higher. In contrast, a significant drop in expression was observed across 15 kinds of cancer, including glioma bile duct carcinoma (refer to Figure SA). With the coxph function, a Cox proportional hazards regression model was utilized to investigate the correlation between gene expression and prognosis across various types of cancer. Prognostic markers were evaluated for statistical significance using the logrank test. Findings revealed that

elevated PCSK9 expression correlated with adverse outcomes in nine types of cancer, whereas a singular cancer type demonstrated that reduced expression was linked to unfavorable prognosis, as shown in Figure Sb. Further, we analyzed clinical data in TCGA-PAAD using an online database (<http://www.linkedomics.org/login.php>). First, we can see that high PCSK9 expression is significantly associated with poor prognosis of patients as seen in Figure S2A. Figure S2B&C show that PCSK9 is related to patient age and tumor residual, the higher the expression of PCSK9 means the more residual tumors. These results indicated that the high expression of PCSK9 was associated with the degree of more malignant pancreatic cancer. Although there was no significant difference between PCSK9 expression and histological type, T and N stages,

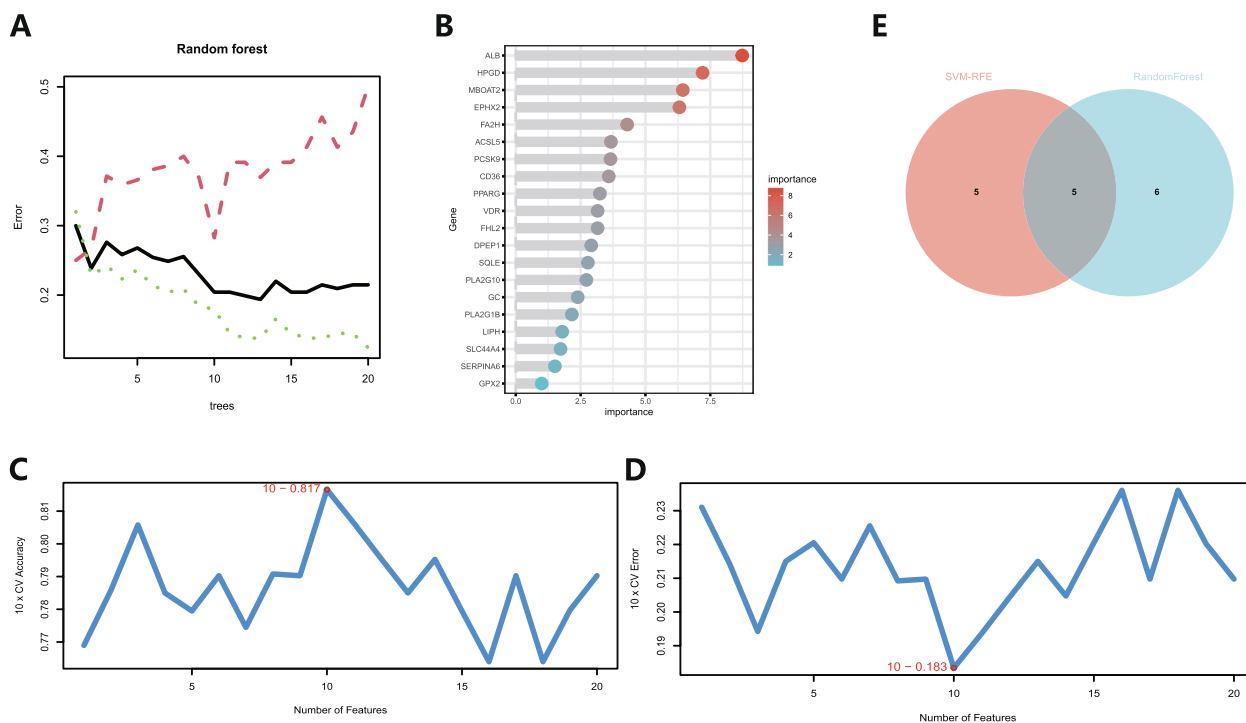


**Fig. 2** Using machine learning to screen possible biomarkers for PC. **A,B** The random forest algorithm illustrates the inaccuracy in PC; the control group and genes are prioritized according to their importance score. **C,D** Plots of biological marker screening using SVM-RFE arithmetic. **E** The Venn diagram depicts the identification of five possible diagnostic genes using the two algorithms described above

it could be seen from Figure S2D-F that higher expression of PCSK9 is most common in pancreatic ductal adenocarcinoma. PCSK9 high expression was more abundant in advanced tumor grade (T3) and the presence of lymphatic metastases (N1). These also suggested that high expression of PCSK9 is associated with PAAD's malignant progression.

**PCSK9 its correlation with ICI levels**

Immune cells, integral to the tumor microenvironment, act as independent prognostic indicators for patients. To delve deeper into the association between PCSK9 levels and ICI status in PC versus normal patients, we utilized the CIBERSORT method with a deconvolution algorithm to evaluate the relative ICI proportions in both tumor and normal groups from GSE71729. Figures 4A-B depict the distribution and relationships of immune cells in tumor versus normal groups. Significant disparities in the prevalence of memory B cells, resting CD4 memory T cells, gamma delta T cells, activated NK cells, Monocytes, M0 macrophages, resting DC, and activated DC between tumor and normal tissues are highlighted in Fig. 4C. Additionally, we further explored the relationship between PCSK9 expression and the level of immune infiltration cells, as shown in Fig. 4D. These results uncover a linkage between PCSK9 and several immune cell types,

including CD8+ T cells, resting CD4+ memory T cells, and M0 macrophages. Collectively, these findings suggest a profound association between PCSK9 and ICI in PC, which may be critical in the modulation of cancer progression through these specific immune cells. To explore the interaction of PCSK9 with immune cells in tumors, we further selected the GEO dataset GSE15471 as well as the TCGA-PAAD data for analysis. As shown in Fig. 4E&F, high expression of PCSK9 in tumors was associated with high Treg cell infiltration. Figure 4G shows that the expression of PCSK9 in the GSE15471 and TCGA-PAAD databases is positively correlated with the infiltration of Treg cells. Further, we performed multicolor fluorescence staining on clinical specimens with high and low expression of PCSK9 (Fig. 4H) and showed that there were more Treg cells (CD4+FOXP3+) in pancreatic cancer tumors with high PCSK9 expression.

**The effects of PCSK9 knockdown on PC cell growth and metastasis in vitro**

Initially, we first explored at the expression of PCSK9 protein in 32 pancreatic cancer tissues in this work. According to Fig. 5A, PCSK9 protein was predominantly more highly expressed in tumor cells than in the corresponding neighboring normal tissues and distant tissues. However, it was discovered that the expression

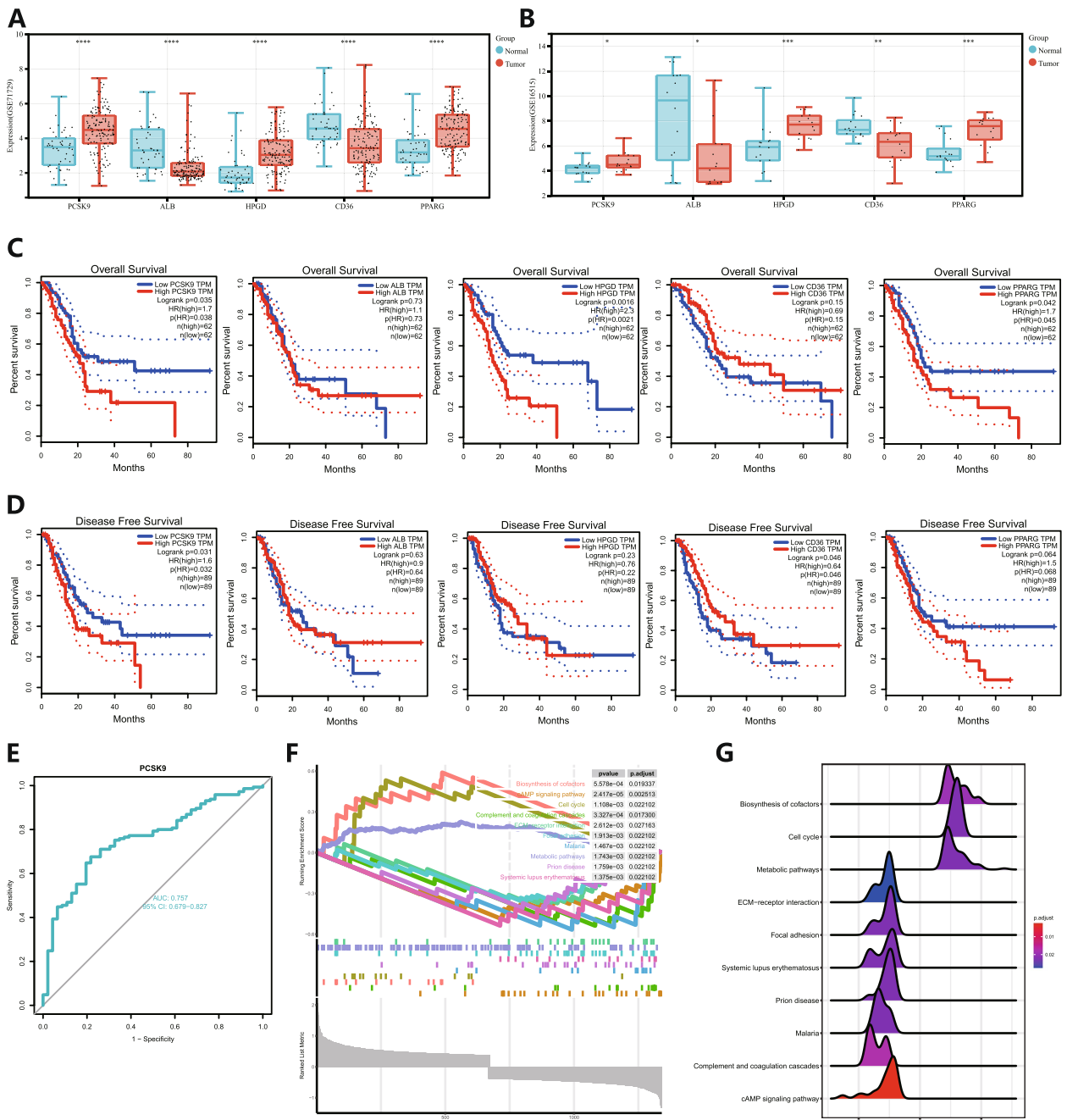


**Fig. 3** Identification and validation of the major gene signature of PCSK9 in PAAD. **A,B** Expression differences in five genes between tumor and normal tissues in GEO datasets. **\*\*\*** $P < 0.001$ , **\*\*** $P < 0.01$ , **\*** $P < 0.05$ . **C,D** OS and DFS analysis of five genes on PC using the GEPIA2 database. **E** The ROC curve for PCSK9. **F,G** Ridge plot and line graph from the GESA study of PCSK9

(See figure on next page.)

**Fig. 4** Comparison of ICI in PC and Normal Tissue. **A** A bar plot depicts the distribution of 22 types of immune cells across different samples. **B** A schematic illustrating the relationship between the 22 immune cell types. **C** A violin plot compares the proportions of 22 immune cell types in PC with normal tissue. **D** A graph depicts the relationship between PCSK9 expression and ICI in both PC and normal samples. **E&F** A violin plot compares the proportions of 22 immune cell types in PC with different expression of PCSK9 in GSE15471 and TCGA-PAAD databases. **G** Correlation between PCSK9 expression and Treg infiltration. **H** mIHC showed the Treg infiltration in different PCSK9 tissue samples

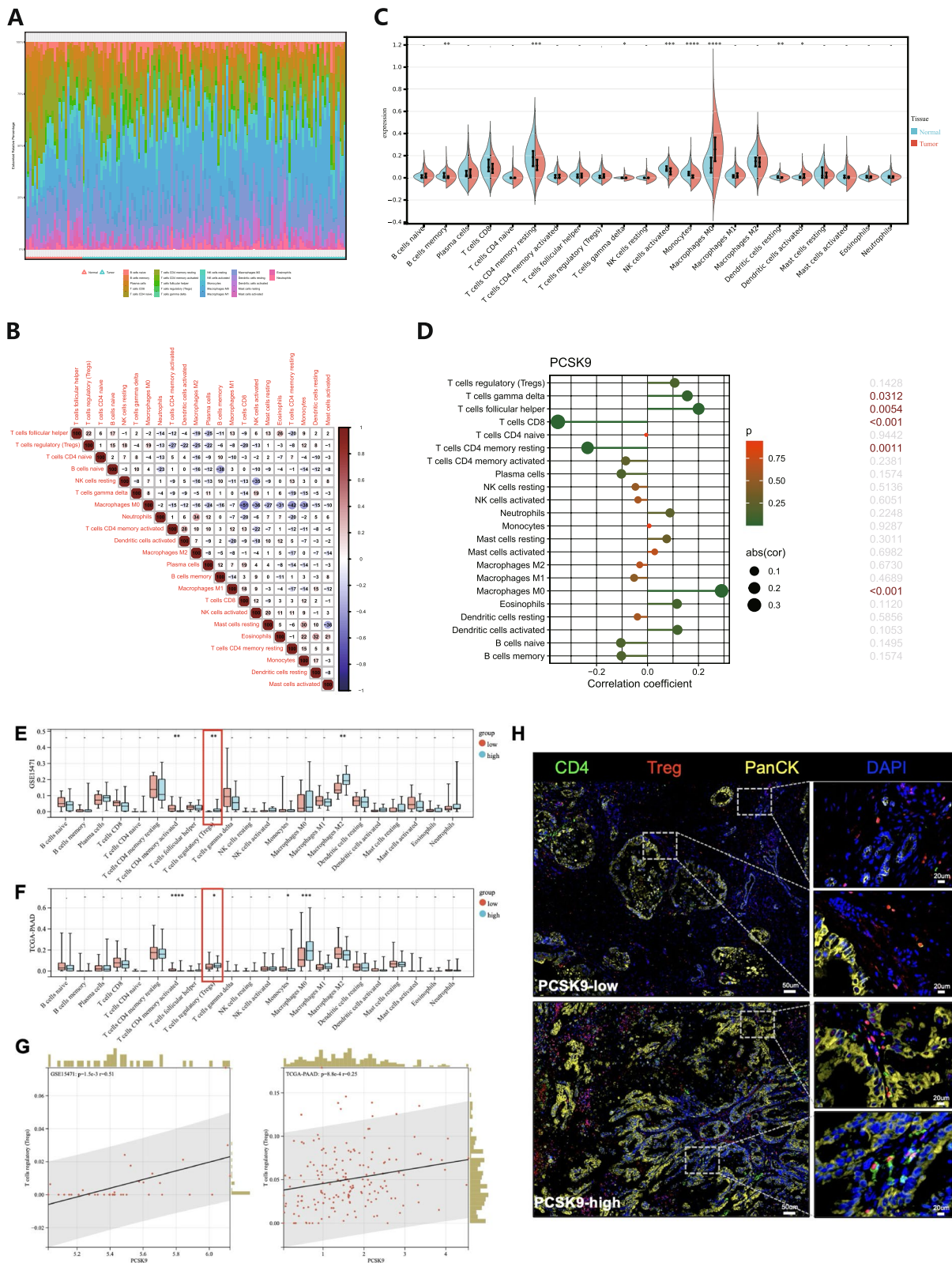


**Fig. 4** (See legend on previous page.)

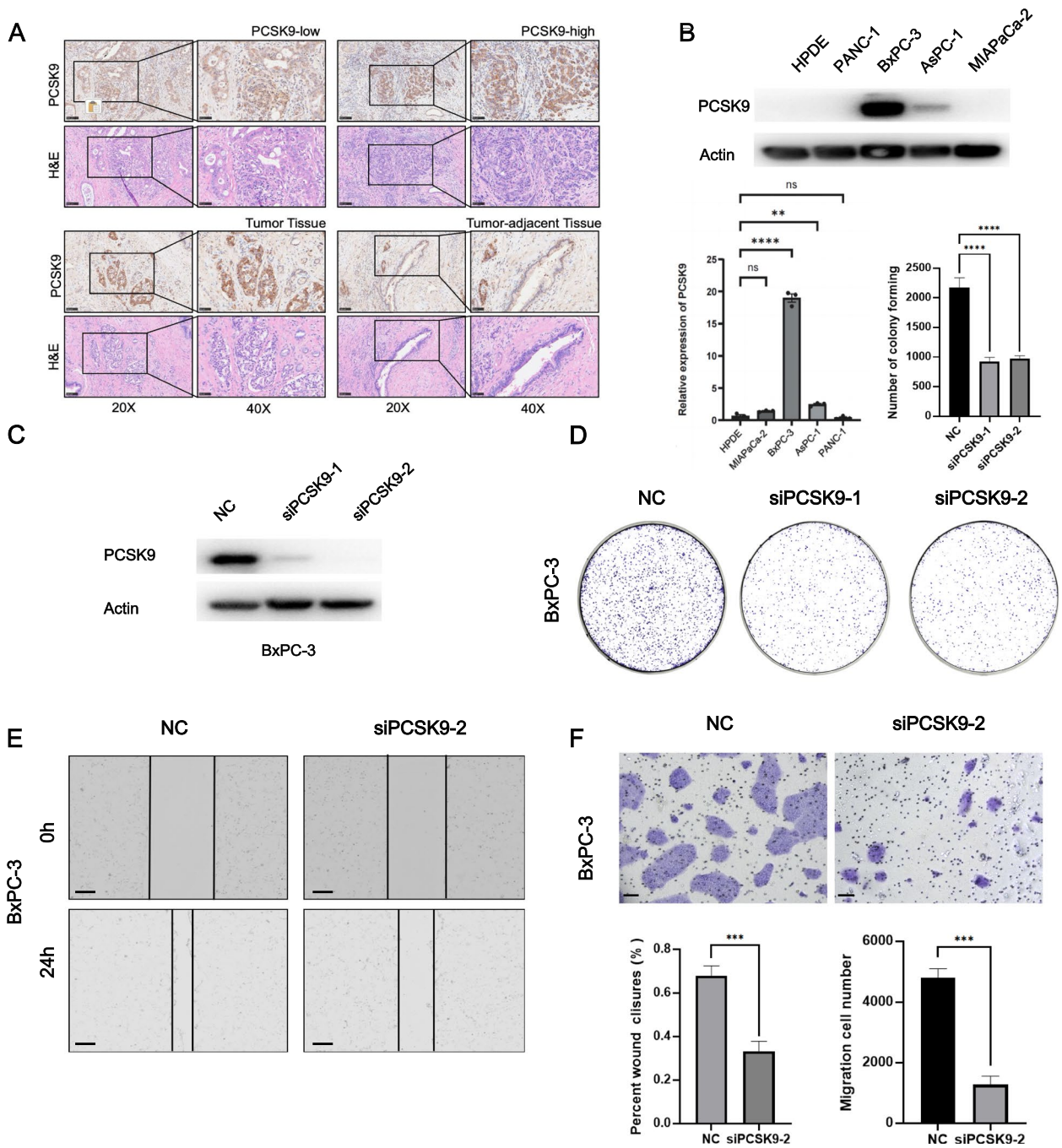


**Fig. 5** Elevated PCSK9 Expression in Human PAAD Cell Lines and Tissues, with Insights into PCSK9's Impact on PAAD Cell Growth and Movement. **A** IHC and H&E staining exhibits both weak and strong PCSK9 expression in normal and tumor tissues from three individuals. Scale bar: 20X-100  $\mu$ m, 40X-50  $\mu$ m. **B** Comparative analysis of PCSK9 expression in HPDE normal pancreatic epithelial cells and various PC (PC) cell lines **C** Western blot analysis of PCSK9 expression in BxPC-3 cells. **D** A colony-formation assay demonstrates the effect of PCSK9 silencing (siPCSK9-1 and siPCSK9-2) on the proliferative capacity of BxPC-3 cells. **E** Wound-healing assays reveal the reduced migratory ability of BxPC-3 cells subjected to siPCSK9-2 treatment for 72 h. Scale bar: 200  $\mu$ m. **F** Transwell assays quantify the decrease in migration and invasion capabilities of PC cells following 72-h siPCSK9 treatment. Scale bar: 100  $\mu$ m

levels of PCSK9 in the nearby and distant tissues were comparable. The expression levels of the PCSK9 protein were measured in the HPDE normal pancreatic epithelial cell line and multiple PC cell lines, demonstrating that PCSK9 expression in PC cell lines was much higher compared to HPDE, as shown in Fig. 5B. Further to investigate the effect of PCSK9 on PC cells in vitro, we transiently transfected negative control (NC) siRNA and PCSK9 siRNA into BxPC-3 cells having very high expression of PCSK9, respectively. Meanwhile western blot was conducted to confirm the decrease in PCSK9 protein expression. To evaluate the functional implications of PCSK9, assays for cell colony formation, wound healing, and transwell migration of tumor cells were conducted. As were indicated by cell colony formation assay, Knockdown of PCSK9 substantially diminished the viability of BxPC-3 cells after transient transfection (all  $p < 0.05$ ), as demonstrated in Figs. 5C. Moreover, the wound-healing assays and transwell data revealed that PCSK9 knockdown reduced the capacity of BxPC-3 cell migration in Fig. 5D&E. These results suggest that PCSK9 was responsible for PC cells growth and metastasis in vitro.

**PCSK9's role in promoting PC proliferation in vivo**

Utilizing lentiviral particles carrying PCSK9 shRNA to infect cells, we obtained stable PCSK9 knockdown sub-lines to further verify our findings. To corroborate our in vitro observations, the oncogenic potential of PCSK9 was evaluated in vivo by implanting BxPC-3 cells subcutaneously into a xenograft mouse model. Two groups of mice were formed: a control group (shRNA-NC) and one that had been treated with shRNA-PCSK9. Then, we extracted total protein from fresh tumors. Western blot revealed that the expression of PCSK9 was significantly downregulated in shRNA-PCSK9-treated mice, as shown in Fig. 6A. As depicted in Figs. 6B&D, compared to mice in the control group, the volume and weight of the tumors in shRNA-PCSK9-treated mice were drastically reduced. To evaluate the expression of PCSK9 and Ki-67 in two groups, we conducted IHC and the results revealed that the expression of PCSK9 and Ki-67 were obvious inhibited after knockdown of PCSK9 in Fig. 6C&E. This suggests that knockdown of PCSK9 can inhibit the proliferative ability of PC in vivo.

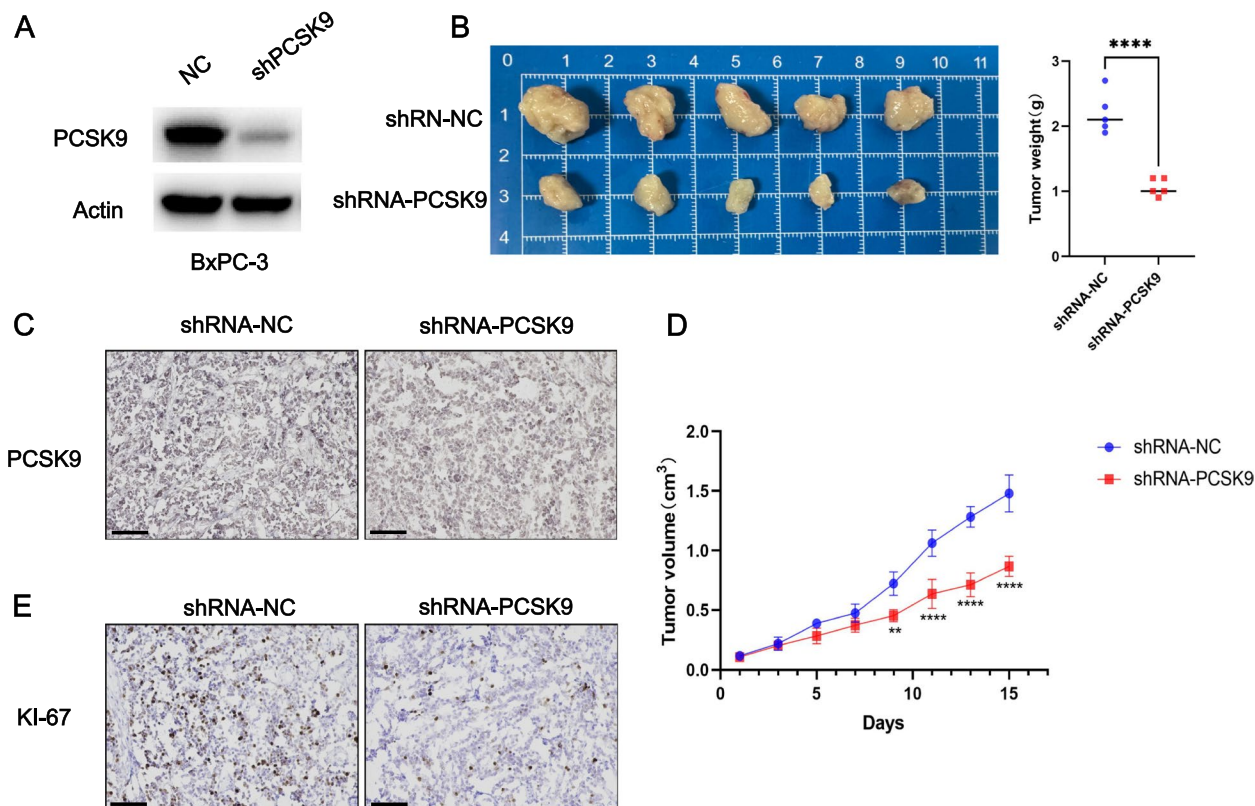


**Fig. 6** PCSK9's Role in Modulating PC Proliferation In Vivo. **A** Western blot analysis of PCSK9 expression in BxPC-3 cells. **B** Ten mice were divided into two groups, receiving treatments with shRNA-NC and shRNA-PCSK9, respectively. Post-euthanasia, the excised tumors were photographed. And a systematic record of each mouse's body weight was kept throughout the study period. **D** The tumor volumes extracted from each mouse were measured precisely. **C, E** IHC staining showed the expression of PCSK9 and Ki-67 in the tumor tissues from two groups. Scale bar: 250  $\mu$ m

## Discussion

PAAD is identified as a highly malignant tumor. The lack of early symptoms, swift disease advancement, low surgical resection rate, and suboptimal chemotherapy response all contribute to the generally dismal prognosis for patients [19]. The increased availability of high-throughput sequencing data has contributed in the identification of a growing number of biomarkers for diagnosing and treating PC. This cancer is characterized as a heterogeneous condition, impacted by genetic variability, hypoxic environments, and metabolic reprogramming [20]. The worth of lipid metabolism in the inception and development of PAAD is gaining recognition [6]. Nonetheless, perhaps owing to an incomplete grasp of the genetic makeup and energy provision mechanisms specific to PAAD, research into genes associated with lipid metabolism within this domain remains inadequately thorough. Consequently, to bridge this gap, we amalgamated PC GEO datasets with gene sets pertinent to lipid metabolism, undertaking an extensive bioinformatic evaluation. This strategy seeks to pinpoint novel characteristic genes to assist in diagnosing and treating patients with PC, a notably aggressive tumor of the digestive tract.

In our study, we first compared 145 pancreatic and 46 normal pancreatic tissues in the GEO dataset GSE71729, identifying 455 significantly different genes. By intersecting these genes with a lipid metabolism gene set, we obtained a total of 20 overlapping genes. Utilizing two machine learning algorithms with the aforementioned 20 genes, we identified five key genes (PCSK9, ALB, HPGD, CD36, PPARG). Survival analyses conducted on these genes, utilizing the GEPIA database, revealed that PCSK9 showed statistically significant disparities in OS and DFS among patients. Additionally, we found that PCSK9 was in association with immune infiltration of CD8 T cells, B cells, and macrophages in pancreatic cancer. Studies in other tumors, such as colorectal cancer [18], have found that deletion or suppression of PCSK9 in tumor cells can inhibit tumor progression by enhancing anti-tumor immunity through enhanced CD8 T cell activity. But in pancreatic cancer, the correlation between PCSK9 and immune infiltration has not been reported. Our findings suggest that PCSK9 may be applied as a new immunotherapeutic target with pancreatic cancer. Although this study has not validated the relevant findings, we will continuously conduct relevant experiments for excavation and validation in the future. PCSK9, identified as the ninth entity in the proprotein convertase family, primarily functions via its engagement with cell membranes. This engagement promotes the degradation of low-density lipoproteins, thereby regulating the concentrations of plasma LDL. Variations in the PCSK9 gene have been

linked to autosomal dominant familial hypercholesterolemia. Despite this, the expression patterns and specific contributions of PCSK9 in the context of PAAD are not completely understood.

## Conclusion

For the first time, our team demonstrates that PCSK9 expression levels varied between PC and normal samples. Furthermore, ROC analysis verified PCSK9's strong capacity to differentiate PC from normal samples. Importantly, we discovered that PCSK9 expression was considerably elevated in PC cell lines and tissues. Furthermore, our findings show that PCSK9 promotes tumor cell proliferation and migration, pointing to its prospects as a therapeutic target in advanced PAAD treatment.

## Supplementary Information

The online version contains supplementary material available at <https://doi.org/10.1186/s12957-024-03532-0>.

Supplementary Material 1: Figure S1. PCSK9 Expression and Prognosis Across Multiple Cancer Types. (A) PCSK9 expression was found to be elevated in 16 out of 34 cancer types when compared to normal tissues. (B) A forest plot illustrating the prognostic analysis of PCSK9 across various cancer types.

Supplementary Material 2: Figure S2. Correlation between PCSK9 expression and clinical consequences of pancreatic cancer. (A) Correlation between PCSK9 expression and overall survival. (B) Correlation between PCSK9 expression and patients' age. (C) Correlation between PCSK9 expression and residual tumor. (D) Correlation between PCSK9 expression and histological type. (E) Correlation between PCSK9 expression and T stage. (F) Correlation between PCSK9 expression and N stage.

## Acknowledgements

Not applicable.

## Authors' contributions

XL and XZ conceived and designed the experiments; SZ, QG and AC performed the experiments; QG and AC analyzed the data; XL and XZ contributed reagents/materials/analysis tools; SZ and QG wrote the paper. All authors read and approved the final manuscript.

## Funding

The authors declare that no funds, grants, or other support was received during the preparation of this manuscript.

## Availability of data and materials

All data generated or analyzed during this study are included in this article. The original data can be provided by the corresponding author upon reasonable request.

## Data availability

No datasets were generated or analysed during the current study.

## Declarations

### Ethics approval and consent to participate

This study was approved by the ethics committee of Jiangsu University of Medical Sciences under the approved code IR.SUMS.REC.

### Consent for publication

Not Applicable.

**Competing interests**

The authors declare no competing interests.

**Author details**

<sup>1</sup>Department of Gastroenterology, Nanjing Drum Tower Hospital Clinical College of Jiangsu University, Nanjing 210008, China. <sup>2</sup>Department of Gastroenterology, Nanjing Drum Tower Hospital, The Affiliated Hospital of Nanjing University Medical School, No. 321, Zhongshan Road, Nanjing 210008, Jiangsu Province, China.

Received: 19 July 2024 Accepted: 9 September 2024

Published online: 28 September 2024

**References**

- McGuigan A, Kelly P, Turkington RC, Jones C, Coleman HG, McCain RS. Pancreatic cancer: A review of clinical diagnosis, epidemiology, treatment and outcomes. *World J Gastroenterol.* 2018;24(43):4846–61.
- Siegel RL, Miller KD, Wagle NS, Jemal A. Cancer statistics, 2023. *CA Cancer J Clin.* 2023;73(1):17–48.
- Rahib L, Smith BD, Aizenberg R, Rosenzweig AB, Fleshman JM, Matrisian LM. Projecting cancer incidence and deaths to 2030: the unexpected burden of thyroid, liver, and pancreas cancers in the United States. *Cancer Res.* 2014;74(11):2913–21.
- Yang J, Xu R, Wang C, Qiu J, Ren B, You L. Early screening and diagnosis strategies of pancreatic cancer: a comprehensive review. *Cancer Commun (Lond).* 2021;41(12):1257–74.
- Vander Heiden MG, DeBerardinis RJ. Understanding the intersections between metabolism and cancer biology. *Cell.* 2017;168(4):657–69.
- Sunami Y, Rebelo A, Kleeff J. Lipid metabolism and lipid droplets in pancreatic cancer and stellate cells. *Cancers (Basel).* 2017;10(1):3.
- Bacci M, Lorito N, Smiraglia A, Morandi A. Fat and furious: lipid metabolism in antitumoral therapy response and resistance. *Trends Cancer.* 2021;7(3):198–213.
- Luo X, Cheng C, Tan Z, Li N, Tang M, Yang L, Cao Y. Emerging roles of lipid metabolism in cancer metastasis. *Mol Cancer.* 2017;16(1):76.
- Byrne A, Savas P, Sant S, Li R, Virassamy B, Luen SJ, et al. Tissue-resident memory T cells in breast cancer control and immunotherapy responses. *Nat Rev Clin Oncol.* 2020;17(6):341–8.
- Butler LM, Perone Y, Dehairs J, Lupien LE, de Laat V, Talebi A, et al. Lipids and cancer: Emerging roles in pathogenesis, diagnosis and therapeutic intervention. *Adv Drug Deliv Rev.* 2020;159:245–93.
- Gomaschi M. Role of Lipoproteins in the Microenvironment of Hormone-Dependent Cancers. *Trends Endocrinol Metab.* 2020;31(3):256–68.
- Abifadel M, Varret M, Rabès JP, Allard D, Ouguerram K, Devillers M, et al. Mutations in PCSK9 cause autosomal dominant hypercholesterolemia. *Nat Genet.* 2003;34(2):154–6.
- Bonaventura A, Grossi F, Montecucco F. PCSK9 is a promising prognostic marker in patients with advanced NSCLC. *Cancer Immunol Immunother.* 2020;69(3):491–2.
- Zhang SZ, Zhu XD, Feng LH, Li XL, Liu XF, Sun HC, et al. PCSK9 promotes tumor growth by inhibiting tumor cell apoptosis in hepatocellular carcinoma. *Exp Hematol Oncol.* 2021;10(1):25.
- Abdelwahed KS, Siddique AB, Mohyeldin MM, Qusa MH, Goda AA, Singh SS, et al. Pseurotin A as a novel suppressor of hormone dependent breast cancer progression and recurrence by inhibiting PCSK9 secretion and interaction with LDL receptor. *Pharmacol Res.* 2020;158:104847.
- Xu X, Cui Y, Cao L, Zhang Y, Yin Y, Hu X. PCSK9 regulates apoptosis in human lung adenocarcinoma A549 cells via endoplasmic reticulum stress and mitochondrial signaling pathways. *Exp Ther Med.* 2017;13(5):1993–9.
- Xu B, Li S, Fang Y, Zou Y, Song D, Zhang S, et al. Proprotein convertase subtilisin/kexin type 9 promotes gastric cancer metastasis and suppresses apoptosis by facilitating MAPK signaling pathway through HSP70 up-regulation. *Front Oncol.* 2020;10:609663.
- Yuan J, Cai T, Zheng X, Ren Y, Qi J, Lu X, et al. Potentiating CD8(+) T cell antitumor activity by inhibiting PCSK9 to promote LDLR-mediated TCR recycling and signaling. *Protein Cell.* 2021;12(4):240–60.
- Siegel RL, Miller KD, Jemal A. Cancer statistics, 2019. *CA Cancer J Clin.* 2019;69(1):7–34.
- Lyssiotis CA, Kimmelman AC. Metabolic interactions in the tumor micro-environment. *Trends Cell Biol.* 2017;27(11):863–75.

**Publisher's Note**

Springer Nature remains neutral with regard to jurisdictional claims in published maps and institutional affiliations.